We are IntechOpen,
the world's leading publisher of
Open Access books
Built by scientists, for scientists

5,000
Open access books available

125,000
International authors and editors

140M
Downloads

Our authors are among the

154
Countries delivered to

TOP 1%
most cited scientists

12.2%
Contributors from top 500 universities

CLARIVATE ANALYTICS
BOOK CITATION INDEX
INDEXED

WEB OF SCIENCE™

Selection of our books indexed in the Book Citation Index
in Web of Science™ Core Collection (BKCI)

Interested in publishing with us?
Contact book.department@intechopen.com

Numbers displayed above are based on latest data collected.
For more information visit www.intechopen.com

Chapter

The Multiphase Flow CFD Analysis in Journal Bearings Considering Surface Tension and Oil-Filler Port Flow

Masayuki Ochiai, Fuma Sakai and Hiromu Hashimoto

Abstract

This chapter presents the multiphase computational fluid dynamics (CFD) analysis on oil-lubricated high-speed journal bearings considering the oil-filler port. Journal bearings are widely used for high-speed rotating machinery such as turbines, compressors, pumps, automobiles, and so on. They can support the rotating shaft utilizing the oil lubrication film wedge effects used in the bearing clearance. Previously, in the analysis of journal bearings, which clearance is very narrow compared with shaft diameter, the Reynolds equation has been used on journal bearing analysis because of its applicability on the narrow space calculation and its low calculation cost. However, the gaseous-phase area generated in the journal bearing and the effect of oil-filler port cannot be reproduced accurately using the method. Under these backgrounds, some researchers use the CFD analysis to calculate the journal bearing characteristics in recent years. In this chapter, the authors describe the multiphase flow CFD analysis on journal bearing based on our previous studies . At first, the multiphase CFD calculation model on journal bearing and the experimental method are explained. Then, four types of calculation results under flooded and starved lubrication conditions are compared to the experimental ones. Additionally, the effect of surface tension on journal bearing characteristics is discussed. Finally, the CFD thermal analysis results under two types of supply oil conditions are shown.

Keywords: journal bearing, multiphase flow analysis, oil-filler port, cavitation, temperature, stability

1. Introduction

High-speed rotating machinery such as compressors, pumps, gas turbines, and automobiles is used all over the world [1, 2]. Oil-lubricated journal bearings are used widely as a support element of high-speed rotating shafts for reducing friction, enhancing the rotating accuracy. On the journal bearing, many researchers and engineers have been interested in the gaseous phase generated in the bearing clearance, and they tried to predict the existence of the gaseous phase because the bearing characteristics are strongly affected by the gaseous-phase areas. For example, Hashimoto and Ochiai clarified the stability characteristics under starved

lubrication both theoretically and experimentally, and they propose a stabilization method utilizing the starved lubrication [3]. Furthermore, Naruse and Ochiai have experimentally studied the relation between gaseous-phase area and temperature distribution [4]. However, these observations have not been theoretically investigated [5], because the calculation method for the detailed gaseous-phase area has not been proposed. In addition, in actual bearing systems, if the lubricant is not able to supply the bearing sufficiently, it means there are starved lubrication condition and also a high possibility of serious erosion damage or serious seizure on the bearing surfaces. Therefore, it is believed that predicting the gaseous area in journal bearings is very important.

Generally, to analyze the oil-lubricated journal bearing, the Reynolds equation is used, and the half-Sommerfeld condition or the Swift-Stieber condition has been applied [6, 7] in determining the gaseous areas for the Reynolds equation. However, in these models, it is assumed that the negative-pressure areas exist only in the gas phase and there is no oil in the bearing clearance area. Therefore, the flow-rate conservation does not hold in the calculations. As a more advanced method, Coyne and Elrod's condition [8, 9] is used. This model assumes oil-film rupture calculates the surface tension between the oil film and gaseous phase which is ignored in the half-Sommerfeld or the Swift-Stieber conditions. However, it is impossible to estimate the cavitation area of the entire journal bearing including the oil-filler port. Therefore, boundary condition models that consider the cavitation have been studied. For example, Ikeuchi and Mori have analyzed the oil-film cavitation areas while using the modified Reynolds equation [10, 11]. In this method, the two-phase flow is considered as an averaged single-phase flow of oil and gas. However, in the case of high eccentricity ratio and starved lubrication condition, they did not conduct the experimental verification with the cavitation area. On the other hand, considering the finger-type cavitation, analytical methods have been proposed by Boncompine et al. [12] and Hatakenaka et al. [13]. However, the estimations of the variation of the gaseous-phase area against the changing of amount of oil lubricant have not been able to for bearing engineers or researchers. Furthermore, it is reported by Hashimoto, Ochiai, and Sakai that the oil-filler port and supply oil quantity affect the journal bearing characteristics [14, 15]. However, the internal flow of the oil-filler port has not been mentioned specifically. Therefore, a different approach is required to analyze the journal bearing while considering the internal flow of an oil-filler port.

The computational fluid dynamics (CFD) treating a two-phase flow has been proposed [16] recent years. The volume of fluid (VOF) method has the advantage of convergency and calculation times comparing with other methods [17]. Moreover, the VOF method also has the merit of reproducibility of slag flow in journal bearings. Therefore, there are some studies treating a two-phase flow CFD analysis utilizing the VOF method. For example, Zhai et al. and Dhande et al. [18, 19] studied the effect of vapor pressure and rotational speed on the gaseous-phase area of a journal bearing.

However, the experimental verifications have not been done in this study. On the other hand, a combination of the Reynolds equation and CFD analysis considering the two-phase flows was reported by Egbers et al. [20]. Furthermore, the gaseous-phase area in the oil-filler port and the opposite load side that was obtained by the analytical method in this study have been compared with that obtained in the experimental results. However, the analytical results cannot precisely produce the gaseous-phase scale and shape, because the influence of the surface tension has not been calculated.

In this situation, the authors have tried to reproduce the gaseous-phase area on both the bearing surface and the oil-filler port in a small-bore journal bearing under

the flooded and starved lubrication conditions while using a CFD model. Further, effects of VOF, surface tension, and vapor pressure of the setting condition were studied, and these analytical results were compared with the experiment, and the applicability was verified. Then, the authors considered the influence of surface tension on journal bearing from the Weber number, W_e. Furthermore, thermal analysis results under two types of supply oil conditions are shown. The effect of supply oil on bearing temperature characteristics was discussed from the results of calculation and experimental results.

2. Theory and calculation model

As mentioned above, the VOF method has some advantages of calculation cost, convergency, and easy to handle compared with other methods [21–24]. Therefore, the authors selected the VOF method, and actually ANSYS FLUENT 15.0 is used in this study. The used methodology is explained below.

2.1 Governing equations

Instead of the Reynolds equation, we applied the Navier–Stokes equation considering the surface tension to the journal bearing analysis in this study. The mass conservation equation and the momentum equation are shown as follows:

$$\nabla \cdot \vec{u} = 0 \tag{1}$$

$$\rho \left[\frac{\partial \vec{u}}{\partial t} + \nabla \left(\vec{u} \cdot \vec{u} \right) \right] = -\nabla p + \mu \nabla^2 \vec{u} + \rho \vec{g} + \left(\nabla \sigma + \sigma \gamma \vec{n} \right) \delta_{int} \tag{2}$$

where ρ is the fluid density, $\vec{u}$ velocity vector, p fluid pressure, μ fluid viscosity, $\rho \vec{g}$ gravitational force, σ surface tension, $\vec{n}$ normal vector, γ curvature of the boundary surface, and δ_{int} Dirac's delta function.

Moreover, ∇ is a differential operator, defined by

$$\nabla = \left(\frac{\partial}{\partial x}, \frac{\partial}{\partial y}, \frac{\partial}{\partial z} \right) \tag{3}$$

In this VOF calculation model, the fluid density and fluid viscosity are expressed as follows:

$$\rho = F\rho_1 + (1 - F)\rho_2 \tag{4}$$

$$\mu = F\mu_1 + (1 - F)\mu_2 \tag{5}$$

where F is the volume fraction and subscription 1 means oil and 2 means gaseous phase.

This CFD analysis can analyze the internal flow of an oil-filler port with the bearing clearance simultaneously because the inertia term is considered in the basic equation.

On the other hand, the energy equation is shown as follows:

$$\rho c_p \left[\vec{u} \nabla (T) \right] = \lambda \nabla T + S_h + \mu \left(\vec{u} \cdot \nabla^2 \vec{u} \right) \tag{6}$$

where c_p is the specific heat and λ thermal conductivity. Moreover, the second term in the right side means the volume heat term and the third term in the right side means the viscous dissipation term.

2.2 Surface tension and cavitation model

To consider the effect of surface tension, the continuum surface force (CSF) model proposed by Brackbill et al. [25] was used as the surface tension model implemented in FLUENT out-of-the-box. The last term of $\left(\nabla\sigma + \sigma\gamma\vec{n}\right)\delta_{int}$ in Eq. (2) represents the surface tension. In Brackbill et al.'s CSF model, the effect of surface tension is included as the surface tension term in the Navier–Stokes equation.

In addition, the cavitation model proposed by Schnerr and Sauer [20] was also used. The equation for the volume fraction of fluid is as follows:

$$\frac{\partial}{\partial t}(F\rho_2) + \nabla(F\rho_2) = \frac{\rho_1\rho_2}{\rho}\frac{DF}{Dt} \tag{7}$$

The vapor volume fraction ? is related to the number of bubbles n_b per unit volume of liquid and bubble radius R_b as shown in the following equation:

$$F = \frac{n_b \frac{4}{3}\pi R_b{}^3}{1 + n_b \frac{4}{3}\pi R_b{}^3} \tag{8}$$

where n_b is the number of bubbles which was set as 10^{13} in this study.

While considering the vapor pressure, the volume of air that is dissolved in oil expanded caused by a negative pressure which was observed in the journal bearing. Therefore, the vapor pressure was set to zero in this study. Moreover, the flow is laminar, and the analysis was conducted in a steady-state condition.

2.3 Calculation model

Figure 1 depicts the outline of a bearing treating in this study. We chose a full circular-type journal bearing in this study. The upper position of the bearing is provided with an oil-filler port, allowing the lubricating oil to flow into the bearing clearance by using gravity. **Table 1** lists its major dimensions. This model is one of the typical bearings for a small-size rotating machinery.

The model of bearing CFD calculation in this study is depicted in **Figure 2**. The bearing clearance with oil-filler port and oil-supply groove were set as flow calculation regions. The symmetrical configuration against the bearing center is used in reducing the calculation cost. The clearance around the minimum part contains
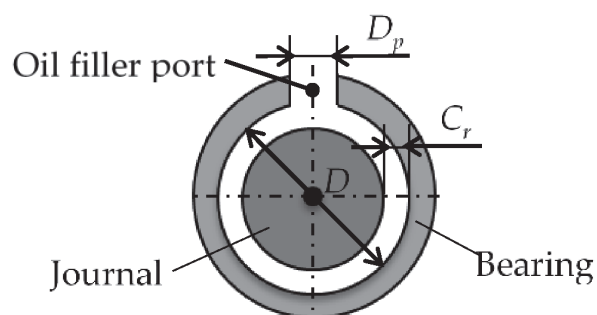

Figure 1.
Geometry of the test journal bearing [1].

Diameter (D) [mm]	25.0
Length (L) [mm]	14.5
Clearance (C_r) [mm]	0.125
Width-diameter ratio (L/D)	0.58
Diameter of oil-filler hole (D_p) [mm]	8.2

Table 1.
Specifications of bearing.
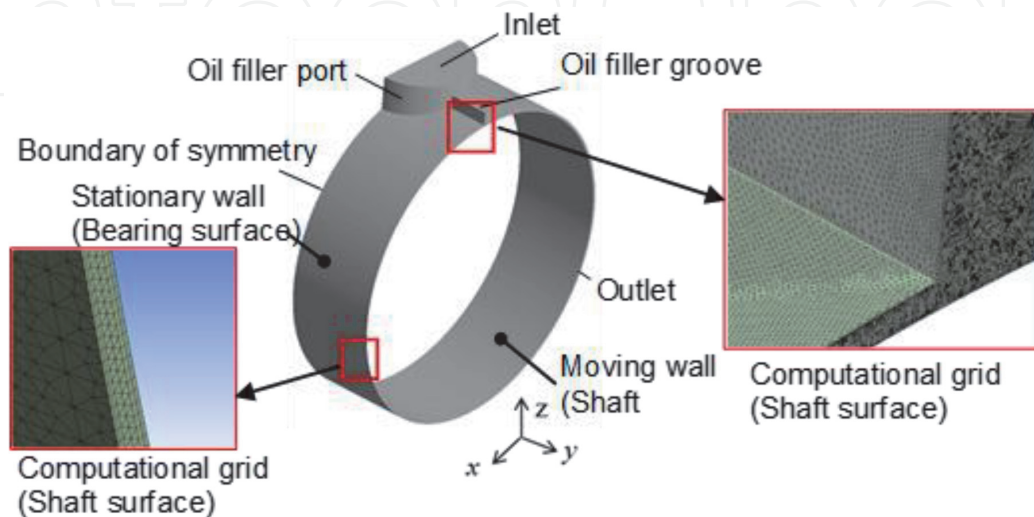
Figure 2.
Calculation model of the journal bearing [1].

Multiphase model			Volume of fluid
Calculation procedure			**Implicit method**
Calculation conditions	Vaporization pressure (P_v) [Pa]		0
	Surface tension (S) [N/m]		0.04
Fluid property	Density (ρ) [kg/m^3]	Oil	860
		Air	1.23
	Viscosity (μ) [Pa·s]	Oil	0.019
		Air	1.75×10^{-5}
	Thermal conductivity (f), [W/m·K]	Oil	0.13
		Air	0.024
	Specific heat (Cp), J/kg·K	Oil	19.5×10^2
		Air	10.1×10^2

Table 2.
Calculation conditions.

six-layer grids in the direction of the bearing clearance. The total mesh number under flooded and starved lubrication conditions were 64×10^5 and 18×10^6, respectively. The confirmation of mesh size was conducted, and enough calculation results were obtained as a pre-test study.

Table 2 shows the calculation conditions. The tension between oil and air was also considered while performing the calculations. The vapor pressure is set zero the same as the ambient pressure. Because, in this study, the side of the bearing and side

of the oil-supply groove are open to the outside, the outside gas is easy to flow into the bearing and easy to generate the gaseous-phase cavitation at the position of negative-pressure generation. The surface tension was set to 0.04 N/m, which was measured while using the du Noüy method (ASTM 971–50).

3. Experiment setup and experimental method

The schematic of the experimental test rig is depicted in **Figure 3**. This rig consists of a rotor installed at its center and a rotating shaft supported by two bearings on its left- and right-hand sides. The right one is the test bearing for visualizations. It is manufactured while using transparent acryl, which allows us to observe the formation of the oil film and the generation of the gaseous phase. The shaft is driven with a DC motor that can control the rotational speed continuously by an inverter. The displacements in the horizontal and vertical directions of the journal are measured with eddy current-type proximity probes. The lubricating oil is supplied from the oil tank positioned on the top of the bearing through a control valve. The leaking oil from the side end of the bearing is returned using the pump. The VG22 oil is used and the oil temperature in the oil tank is fixed to 40°C with a heater.

In this study, we also conducted the measurement of temperature distribution in the journal bearing clearance using sheathed thermocouples. **Figure 4** shows the positions of the thermocouples in the bearing. Two lines of bearing centerline and halfway between the center and side end of the bearing are installed, and they are positioned 45° apart on the bearing's circumference. Moreover, the thermocouples were only installed on one side of the bearing in order to be able to visualize the gaseous phase in the bearing clearance at the same time. It was found in the previous experiments that the temperature measurement error was almost negligible in the case of the obliquely installed thermocouple. The thermocouples were secured by feedthroughs, and oil leakage through the insertion hole was prevented by applying a sealant. As the experimental method, the temperature of the supplied oil was fixed at 40°C, while the rotating speed of the shaft was increased to 7500 rpm. Moreover, the ambient temperature was fixed at 25°C. In this study, the temperature in the bearing clearance was measured under two kinds of supply oil conditions.
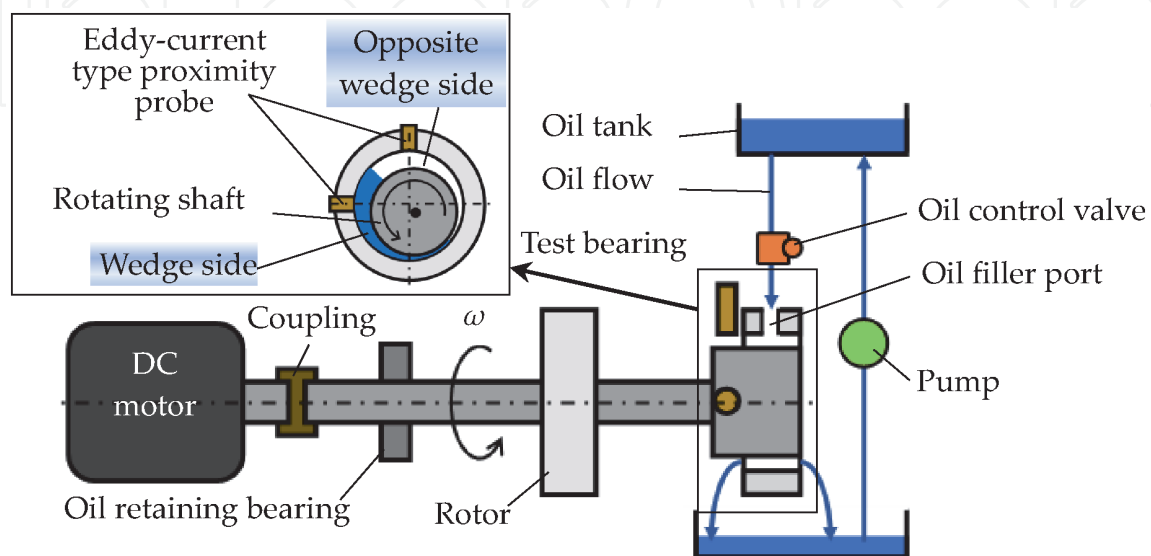

Figure 3.
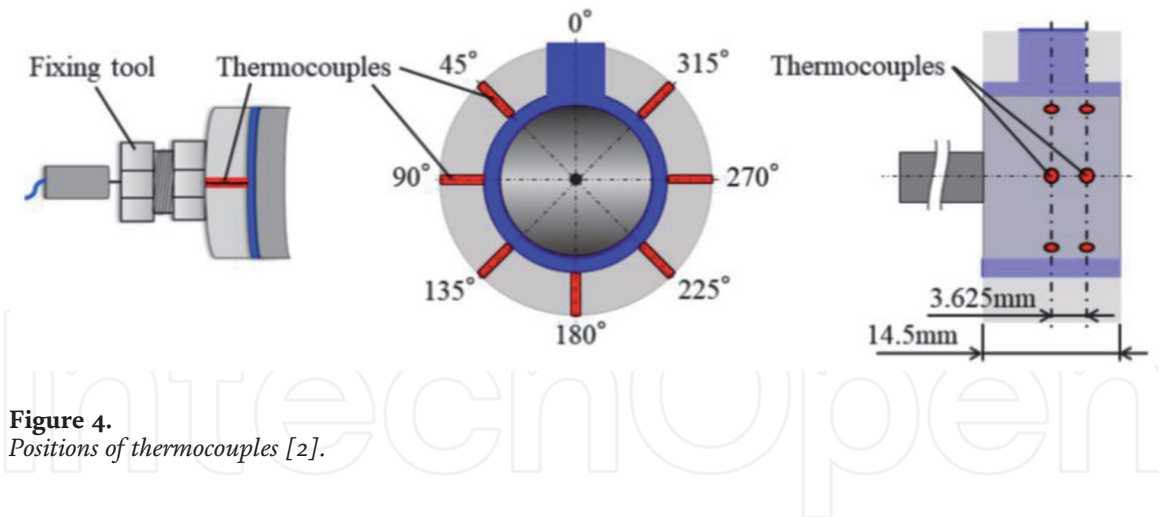*Geometry of an experimental test rig ([1] partially modified).*

Figure 4.
Positions of thermocouples [2].

4. Results and discussions

4.1 Gaseous-phase area reproducibility

4.1.1 Under flooded lubrication conditions in the journal bearing

In this study, four types of calculations were calculated to clarify the effects of vapor pressure and surface tension. Results of (i) analysis of the volume fraction F distribution of oil and (ii) experimental visualization under flooded lubrication conditions are depicted in **Figure 5**. The red color in **Figure 5(i)** indicates the phase of complete oil, whereas the blue color indicates that of complete gas. Further, the solid and dotted black lines perpendicular to the circumferential direction of the bearing indicate the maximum and the minimum clearance, respectively. The 0° means the position of the most upper part of the bearing and the oil-filler port of the bearing exists at this position. The black arrow means the rotational direction and, consequently, the main flow direction of lubrication oil is the same.

In this study, we have presented the results for the surface of the rotating shaft. Moreover, in **Figure 5(ii)** of the experimental result, the yellow areas represent the gaseous phase, and the remaining areas indicate the oil film. The conditions of these calculations and experiment are as shown below. The rotational speed was n = 3500 rpm. The volume of oil supply was q = 2.6 cm^3/s, the eccentricity ratio ε = 0.54, and the attitude angle ϕ = 72.9°. These values are based on the experimental result.

In the case of VOF and VOF with surface tension as shown in **Figure 5(i-a, i-b)**, the volume fraction around the side end of the bearing decreases between 270° and 135°, and the volume fraction of the remaining area is approximately 1, which means complete oil. Around the oil-filler port, the volume fraction is most decreased. In the case of VOF with vapor pressure as depicted in **Figure 5(i-c)**, the volume fraction around the side end of the bearing slightly decreases between 300 and 100°. The range of the volume-fraction decrease in this case is smaller than that observed in the case of VOF alone or in the case of VOF with surface tension. On the other hand, in the case of VOF with vapor pressure and surface tension as shown in **Figure 5(i-d)**, the volume fraction around the bearing side end is approximately 1 between 300 and 0°. This tendency is quite different from other cases. Moreover, between 0 and 135°, the value of volume fraction decreases, and the decreased area which means the gaseous-phase area is wider than that of VOF with vapor pressure shown in **Figure 5(c-1)**. The tendency found in **Figure 5(i-d)** of the gaseous-phase area is also found in the experiment. Therefore, it is concluded that **Figure 5(i-d)** is in good agreement with the experiment compared with the other cases.
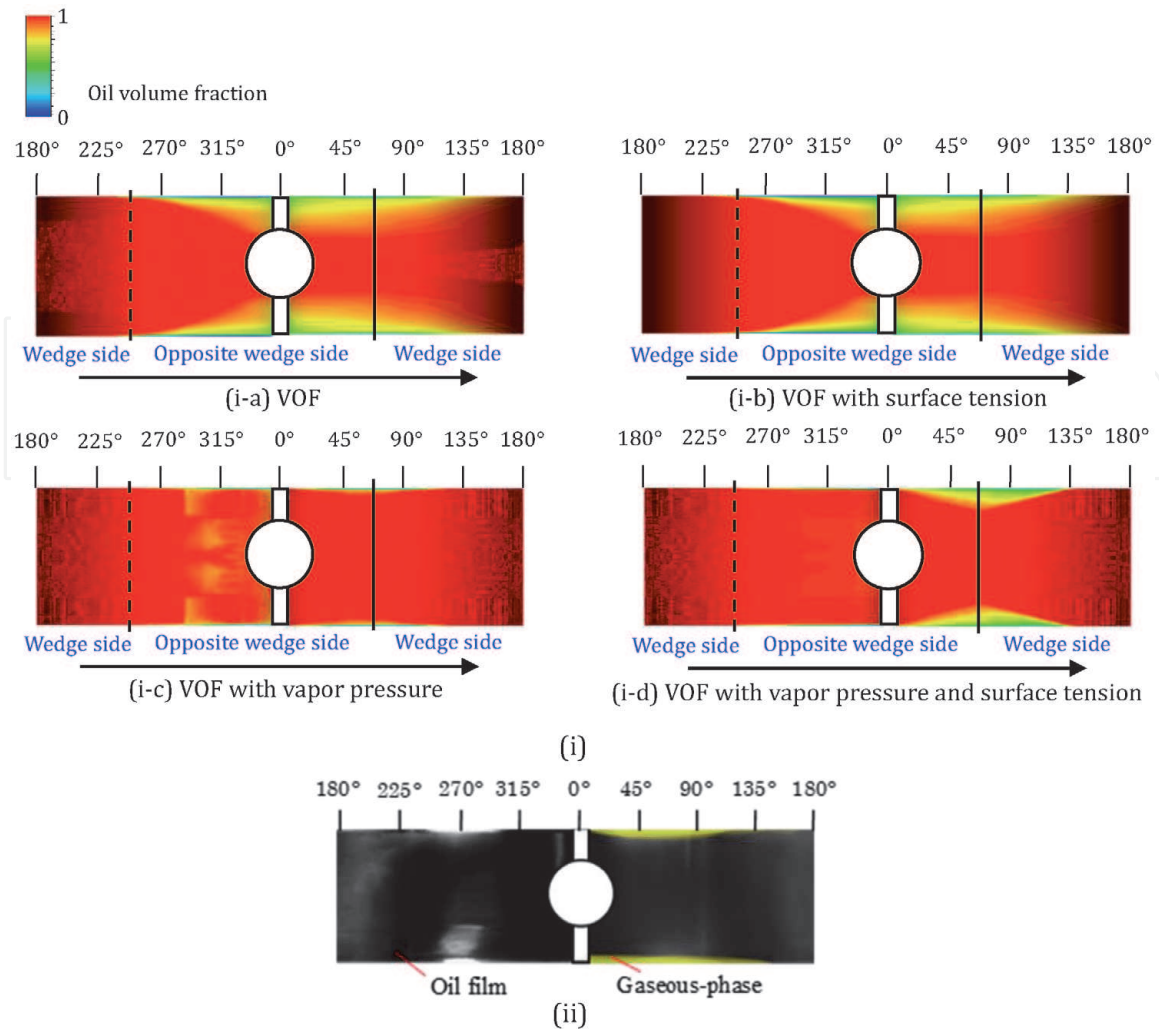
Figure 5.
Comparison of calculation and experimental results under flooded lubrication conditions ([1] partially modified). (i) Calculation results and (ii) Experimental result.

4.1.2 Under starved lubrication conditions in the journal bearing

The calculation results of oil volume fraction and experimental visualization result under starved lubrication conditions are depicted in **Figure 6**. Further, the volume of oil supply under this condition was q = 0.5 cm^3/s, the eccentricity ratio was ε = 0.76, and the attitude angle was ϕ = 71.5°.

From these results, it is found that the volume-fraction distribution and gaseous area under starved lubrication differ from the results under flooded lubrication. In the case of VOF, the volume fraction as shown in **Figure 6(i-a)** is one which means a complete oil phase at the minimum clearance of 180°, and the range of the decrease of volume fraction increases for the remaining ranges. In a wide range of around the side end of the bearing, the volume fraction decreases compared to that of the flooded lubrication conditions.

In **Figure 6(i-b)**, in the case of VOF with surface tension, a similar tendency is observed in the case of VOF. In contrast, from **Figure 6(i-c)**, the volume fraction increases at the side end of the opposite wedge side, and the volume fraction between 0 and 130° decreases at a greater rate than that observed in the cases of VOF and VOF with surface tension. Further, the volume fraction of the opposite wedge is observed to moderately decrease between 180 and 295°.

On the other hand, in the case of VOF with vapor pressure and surface tension shown in **Figure 6(i-d)**, the different tendency is observed. The volume fraction in the vicinity of bearing centerline and side end decreases from 270 to 0°, and
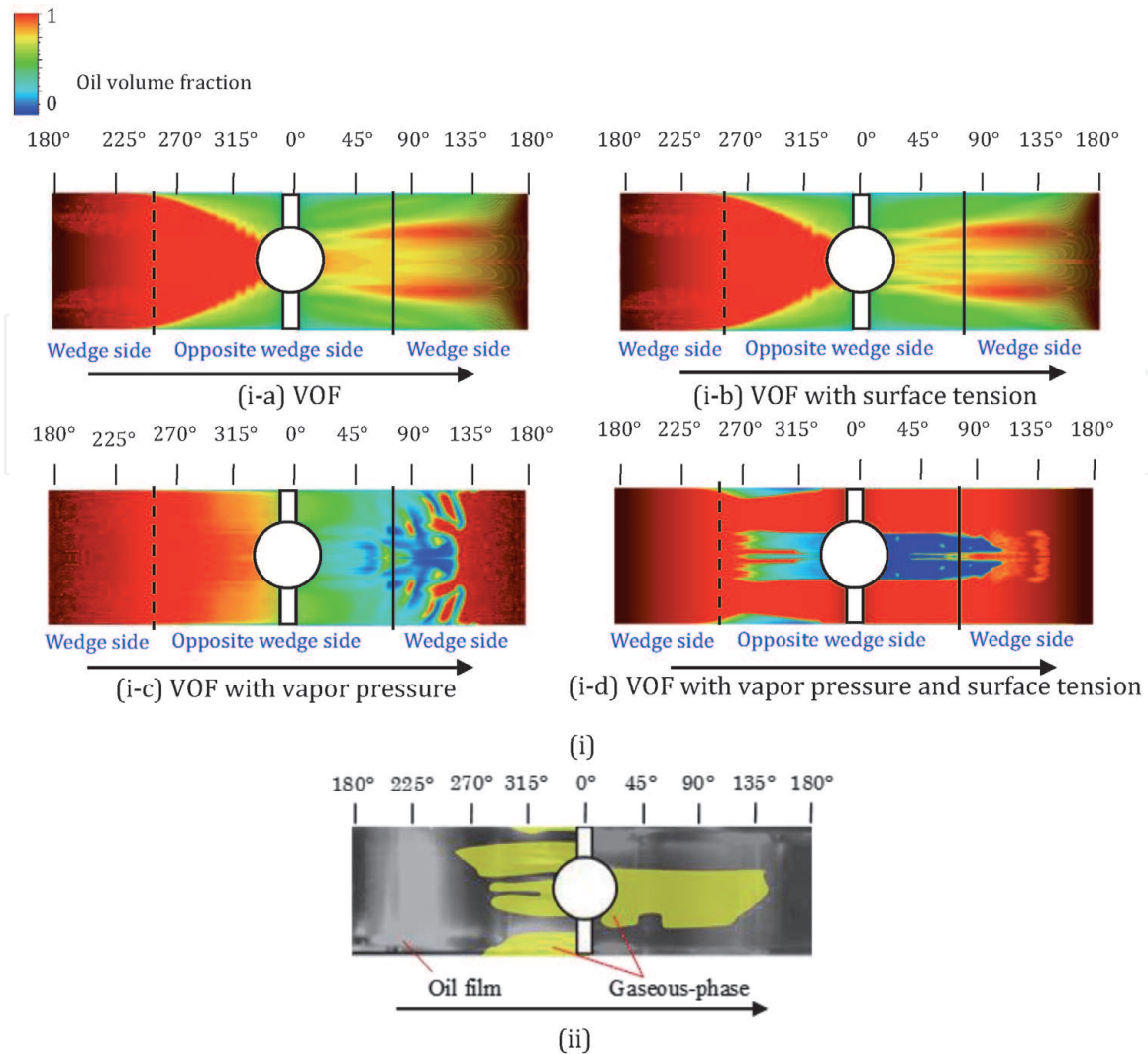
Figure 6.
Comparison of calculation and experimental results under starved lubrication conditions ([1] partially modified). (i) Calculation results and (ii) Experimental result.

between them, striped bands of oil are observed. Additionally, the volume of fraction in the vicinity of the bearing center between 0 and 120° is zero, and this range is observed to be the full air phase. From the above results, it is found that the gaseous phase changes before and behind of oil-filler port.

In the case of VOF with vapor pressure and surface tension as shown in **Figure 6(i-d)**, the tendency of the gaseous-phase area is in good agreement with that of the experiment shown in **Figure 6(ii)**. On the other hand, other calculation results which are shown in **Figure 6(i-a–c)** are very different from the experiment. The differences are more clear than the case of the flooded lubrication condition. Therefore, it is important to consider both vapor pressure and surface tension in the case of starved lubrication conditions especially. From these results, we were interested in the oil-film rupture shape at the end of the wedge side in the case of starved lubrication conditions as shown in **Figure 7**.

Figure 8 depicts the calculation and experimental visualization results of the oil-film rupture under starved lubrication conditions. It is found that the volume fraction near the moving shaft surface is one, and the value is decreasing gradually as approaching the bearing surface in the case of VOF with vapor pressure, as shown in **Figure 8(i-a)**. This tendency is the same as the model of the Coyne and Elrod which define the gas–liquid boundary between the bearing gap. However, in this case, the strong fluctuation is found between the boundaries of the volume fraction.
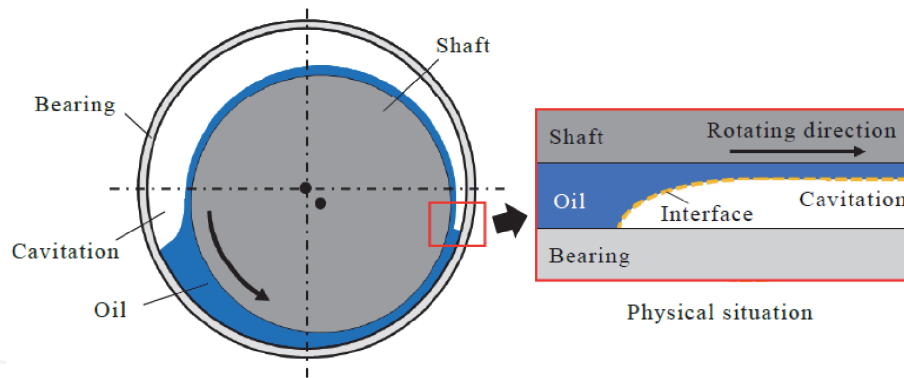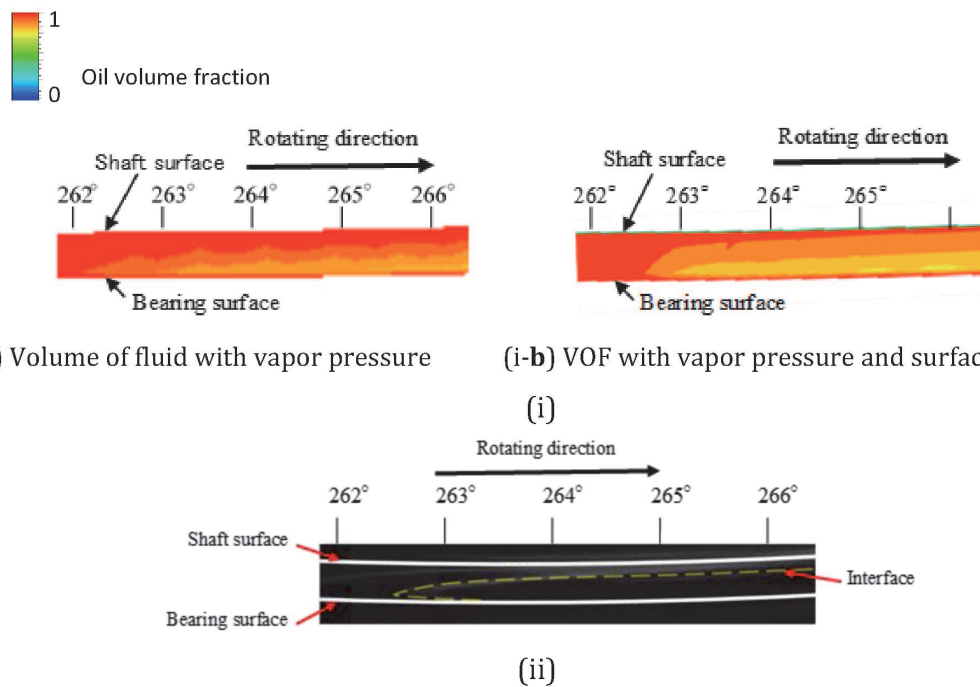
Figure 7.
Oil-film rupture position.

(i-**a**) Volume of fluid with vapor pressure   (i-**b**) VOF with vapor pressure and surface tension

(i)

(ii)

Figure 8.
Calculation and experimental results of the oil-film rupture under starved lubrication [1]. (i) Comparison of calculations and (ii) Experimental visualization result.

In the case of VOF with vapor pressure and surface tension as shown in **Figure 8(i-b)**, a two-phase flow exhibits a similar tendency as that exhibited by VOF with vapor pressure shown in **Figure 8(i-a)**. However, the interface between the oil film and gaseous phase is smoothly curved with an increase in clearance. From these results, it is confirmed that our proposed 3D CFD calculation model considering the vapor and the surface tension can reproduce the oil-gas boundary and it is in good agreement with the experiment shown in **Figure 8(ii)**.

4.2 Inner flow difference on the oil-filler port

From the abovementioned results, we focused on the inner state of the oil-filler port, because the gaseous area around the oil-filler port including the supply groove was large especially under the starved lubrication conditions.

Figure 9 depicts the results at a cross section of the oil-filler port in the case of under flooded lubrication conditions of **Figure 9(a)** and under starved lubrication
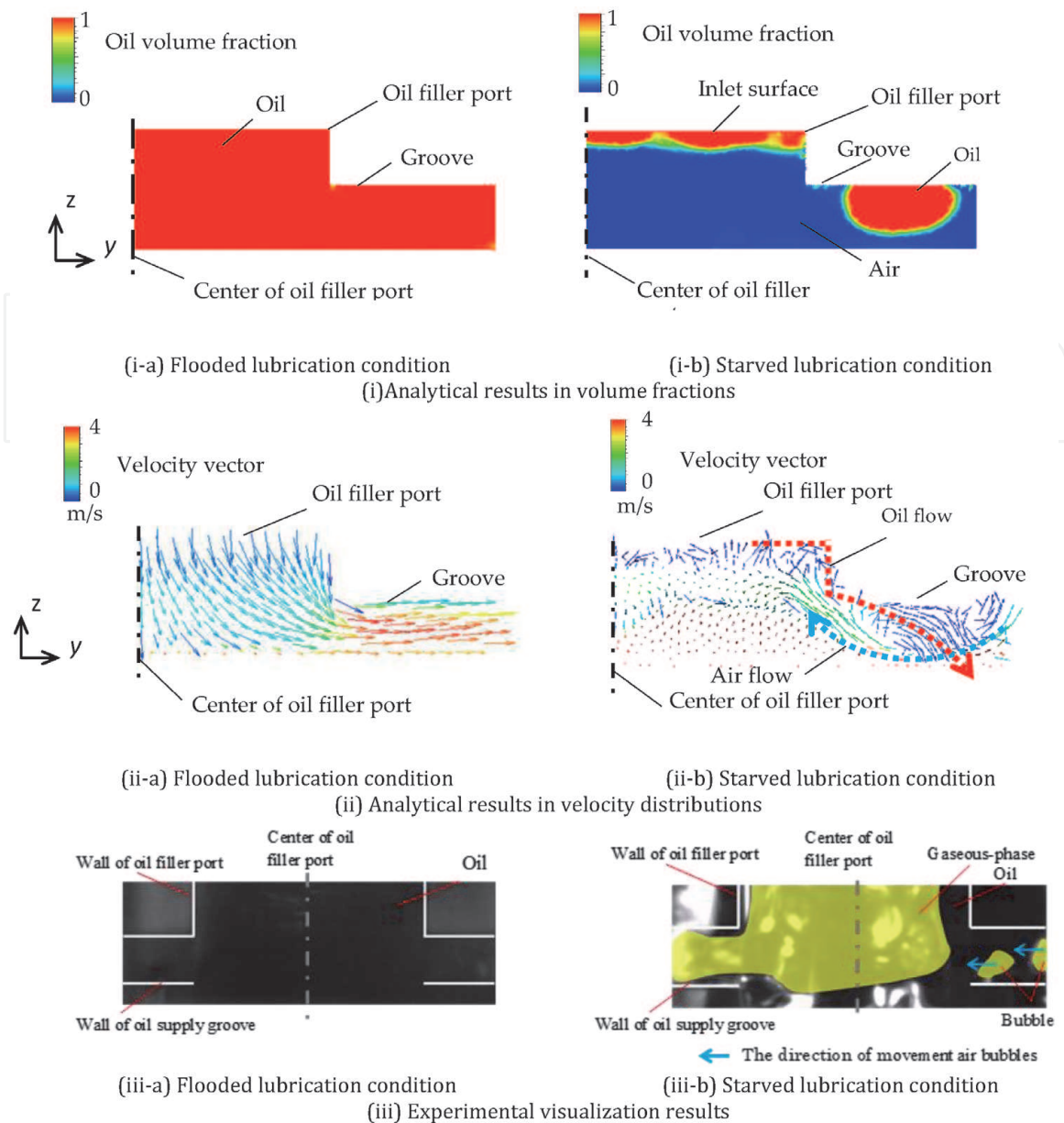
Figure 9.
Results of inner flow on the oil-filler port [1].

conditions **Figure 9(b)**. **Figure 9(i)** indicates the calculation results in volume fraction, **Figure 9(ii)** indicates the calculation results in velocity distribution, and **Figure 9(iii)** indicates the experimental visualization results. These figures depict the view from the front. The dash-dotted lines indicate the surface of symmetry.

From **Figure 9(i-a)**, under flooded condition, the oil phase is observed throughout the structure of the oil-filler port and the oil-supply groove. Furthermore, from **Figure 9(ii-a)**, it is observed that the velocity vectors are directed from the entrance surface of the oil-filler port to the oil-supply groove and bearing clearance in strong momentum. Hence, it is considered to be a less gaseous phase in the bearing clearance under flooded conditions. Here, the comparison between the analytical and experimental visualization results shows that the obtained results are close to the experimental results under the flooded lubrication conditions.

On the other hand, under starved lubrication conditions as shown in **Figure 9(i-b)**, it is observed that the gaseous phase exists in the major area of the oil-filler port whereas the oil exists around the inlet of oil-filler port and at the upper center area of oil-supply groove. Further, from the velocity vector result of **Figure 9(i-b)**, it is found that the oil

flows from the top surface of the oil-filler port to the oil-supply groove along the walls whereas outer air flows into the oil-filler port through the oil-supply groove. One of the main causes of these flows is considered due to the surface tension of oil and air, and the effects appear to be significant especially in the case of starved lubrication.

Furthermore, oil is supplied from the oil-supply groove to the bearing, thereby causing the occurrence of the gaseous phase at the center of the bearing of the wedge side of the journal bearing under starved lubrication conditions.

The same tendencies are confirmed from the experimental visualization results of **Figure 9(iii)**.

4.3 Influence of surface tension in the journal bearing

In the previous section, it is confirmed that considering the surface tension to calculate the gaseous-phase areas accurately in journal bearings especially under starved lubrication is important. In the next step, we considered the influence of surface tension on journal bearing from the viewpoint of Weber number W_e. The Weber number is expressed in the following equation:

$$W_e = \frac{\rho U^2 H}{\sigma} \tag{9}$$

where U represents the speed and H represents representative length.

In the Weber number W_e, the meaning of the numerator is the fluid inertia force and that of the denominator is the surface tension. Generally, it is known that if W_e is less than one, the influence of surface tension is strong.

First, we examined the surface tension influence on bearing clearance. In this case, it was assumed that the representative speed U is the peripheral speed of moving the journal surface. Since the rotational speed is high, the Weber number extremely exceeds, and the influence of surface tension is negligible. This result is reasonable. Because many previous studies have been neglected, the surface tension effect and the reliability have been verified. However, as mentioned above, it is found that the influence of surface tension on gaseous-phase areas under starved lubrication is significant. Therefore, we focused on the internal flow of the oil-filler port. As the representative speed, the internal flow speed which is determined from supply oil flow rate was used.
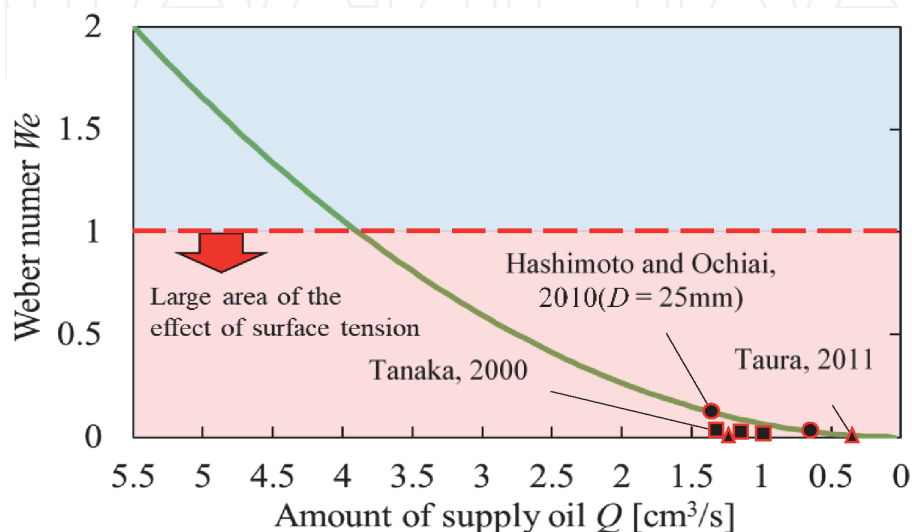

Figure 10.
Relation between the Weber number and amount of supply oil [1].

Figure 10 depicts the calculation result of the Weber number W_e against the oil flow rate. The continuous line indicates the value, whereas several plots indicate the value in other studies of journal bearings under the starved lubrication conditions [3, 26, 27]. Focusing on the continuous line, the Weber number W_e drop below 1 approximately under the amount of supply oil of 4 cm³/s, and the influence of surface tension in the internal flow of the oil-filler port becomes too large to ignore.

Moreover, it is found that the Weber number W_e of another research of journal bearing under starved lubrication is remarkably smaller than one. Therefore, it is concluded that the cause of surface tension influence is related to supply velocity from the oil-filler port.

4.4 Temperature analysis

In this section, the thermal CFD analysis in journal bearing under two kinds of lubrication conditions is discussed. In our previous study [3, 4], it was found that the supply oil quantity affects the journal bearing stability, and the critical oil-supply quantity of transition state is determined. Therefore, two types of oil-supply quantity, one is transition state and the other one is starved lubrication condition, were selected in this chapter. The conditions of supply quantity and journal center positions are shown in **Table 3**. These conditions were decided by the experiment.

4.4.1 Oil-film temperature and volume fraction

Figure 11 shows the thermal CFD analysis results under two conditions of supply oil quantity. **Figure 11(i)** indicates the volume-fraction distribution of oil under both conditions. The red color means full oil and the blue color means full air. **Figure 11(ii)** indicates the analytical results of the temperature distribution of bearing. From **Figure 11(i-a)**, under transition condition, the volume fraction of the wedge side becomes zero at the side end. Thus, these areas are the gaseous phase. Moreover, the volume fraction increases at the centerline of bearing. On the other hand, the volume fraction of the inverse wedge side decreases with increasing of clearance. From **Figure 11(ii-a)**, the temperature slightly rises caused by the shear friction, but it is found that the temperature is almost 40°C at the full area of the bearing. Thus, it is found that the heat quantity by the shear friction is small in the case of the transition region.

On the other hand, from **Figure 11(i-b)**, the volume fraction of the wedge side increases at the center of bearing, while it is zero around the side end. The volume fraction of the inverse wedge side decreases with increasing of clearance, while it becomes zero around the oil-filler port. From **Figure 11(ii-b)**, it is found that the temperature around the oil-filler port is about 38°C while it decreases compared to the temperature of supply oil. Moreover, the temperature of the around centerline on the bearing is smaller compared around the side end.

Figure 12 shows the theoretical results of temperature distribution on the transition region and starved conditions at the point of centerline under (a) transition

	Oil supply amount Q, cm³/s	Eccentricity ε	Attitude angle φ, deg.
Transition region	3.7	0.47	66.9
Starved lubrication	0.5	0.83	43.3

Table 3.
Specifications of calculation conditions [2].

(i-a) Transition $Q = 3.7$ cm³/s   (i-b) Starved $Q = 0.5$ cm³/s

(i) Calculation results in volume fractions

(ii-a) Transition Q = 3.7 cm³/s   (ii-b) Starved $Q = 0.5$ cm³/s
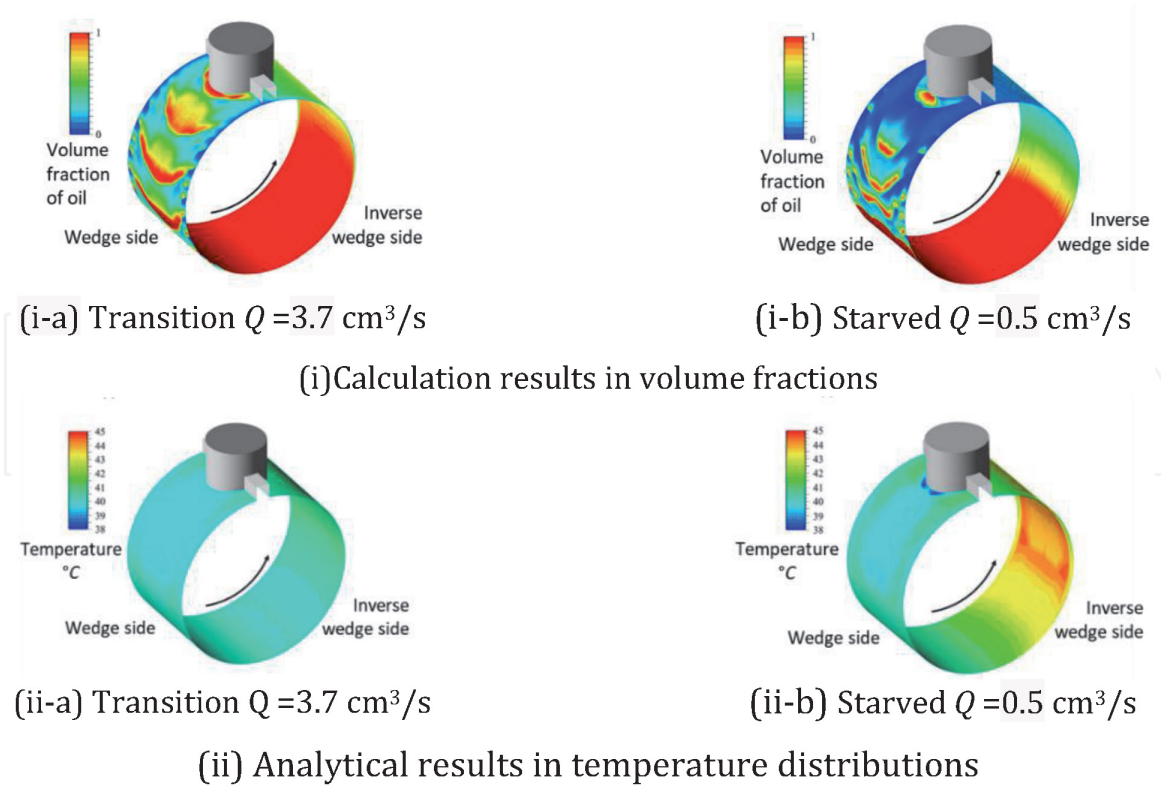
(ii) Analytical results in temperature distributions
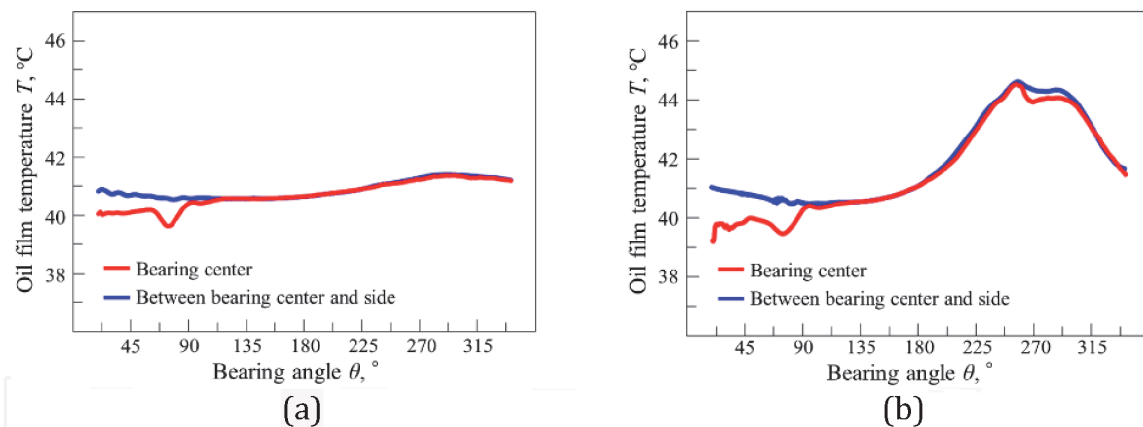
Figure 11.
Results of thermal CFD analysis [2].

Figure 12.
Analytical results in temperature distributions [2]. (a) Transition Q = 3.7 cm³/s and (b) Starved Q = 0.5 cm³/s.

and (b) starved lubrication conditions. From **Figure 12(a)**, the temperature elevation in the bearing clearance against the supply oil temperature which is 40°C is not so high. In addition, there is a little difference from 22.5 to 90°. On the other hand, from the results for the starved lubrication condition, as shown in **Figure 12(b)**, the temperature distributions are extremely different from those of the oil transition conditions. The temperature distributions of the starved lubrication condition increase with an increasing bearing angle after 135°, and the highest temperature area is found around the bearing angle of 250°. This is because the minimum clearance around the bearing angle of 250° decreases and the share friction resistance of oil film rises in the starved lubrication conditions. The temperature difference of the bearing center is found from 22.5 to 90° same as the transition region; however, the amount of difference is larger than that of transition region. Moreover, in the low-temperature region, the value of temperature is lower than the supply oil temperature of 40°C.
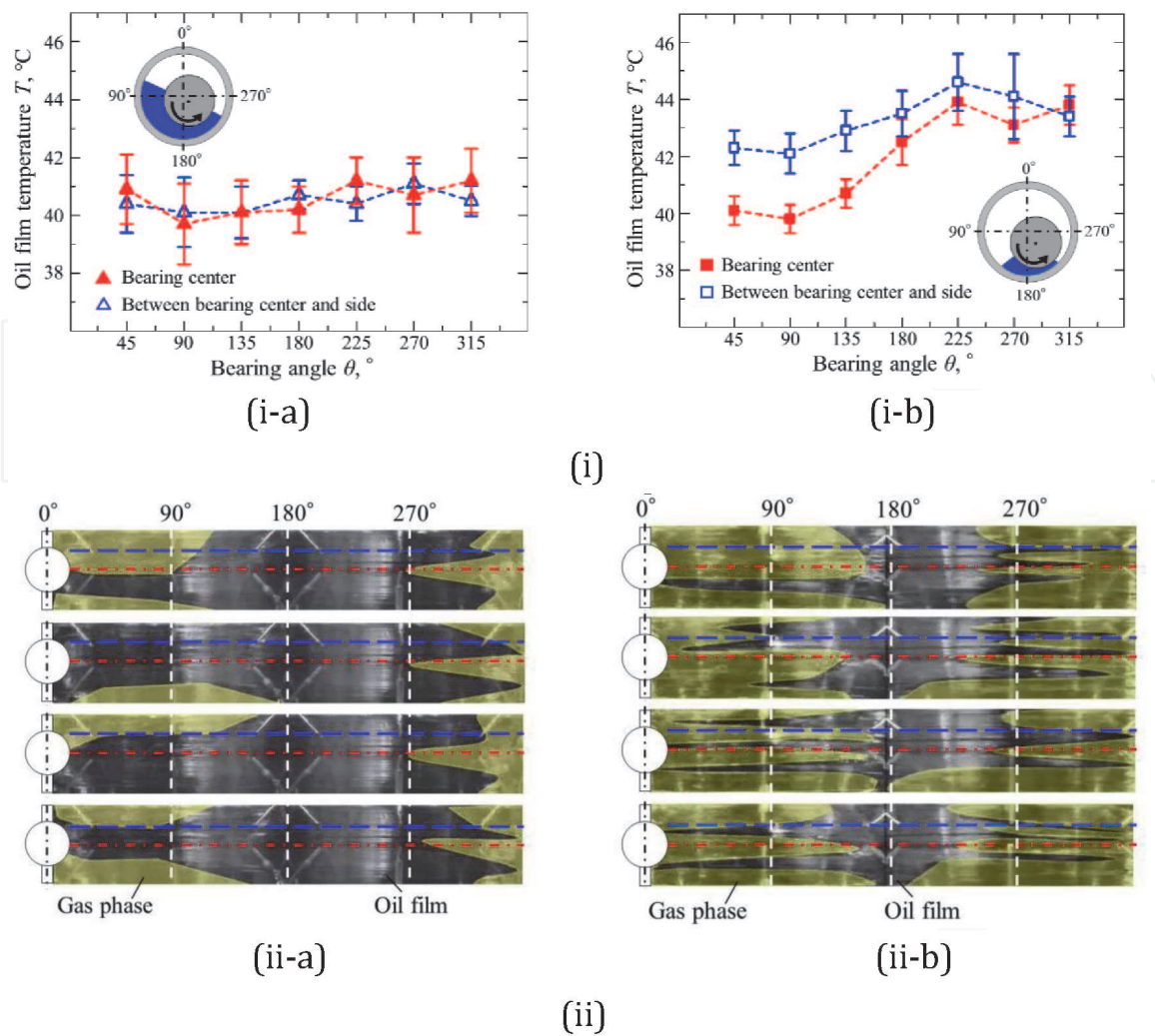
Figure 13.
Results of temperature distributions and gaseous-phase visualizations [2]. (i) Experimental results in temperature distributions ((a) Transition Q = 3.7 cm³/s; (b) Starved Q = 0.5 cm³/s). (ii) Experimental visualization results of gaseous-phase region ((a) Transition Q = 3.7 cm³/s; (b) Starved Q = 0.5 cm³/s).

Figure 13 depicts the experimental visualization results of (i) temperature distributions and (ii) results of gaseous-phase visualization. In **Figure 13(ii-a, b)**, there are typically four results which are indicated due to some fluctuation of gaseous-phase existing under actual rotations.

From the results in **Figure 13(i)**, it is found that the same tendencies of temperature distributions are shown between calculation and experiment. As shown in **Figure 13(i)**, the temperatures are almost constant against the bearing angle in the case of transition condition. Hence, the same tendencies of temperature distributions are found between the calculation and the experiment. On the other hand, under the starved lubrication condition, the temperatures are higher against the bearing angle, and the difference of temperature between two bearing positions is found. Here, the temperature at the center of bearing is lower than that of between the center and side despite being closer to outside the edge. Generally, the temperature of the bearing is larger than that of the side. Therefore, the reason could be the cooling effect from the visualization results shown in **Figure 13(ii)**.

As shown in **Figure 13(ii-a)**, the gaseous phase rarely existed at the center of the bearing at bearing angles between 0 and 135°. However, the temperatures are almost constant. This is because the friction resistance is not so high due to the relatively large amount of oil-film thickness existing in this case.

On the other hand, under starved condition shown in **Figure 13(ii-b)**, the gaseous phase exits at the center of the bearing. The gas is considered the inflow air

from the oil-filler port. Hence, it is believed that the oil film at the center position was cooled down by an inflow air. Comparing with it, the position of between center and side, oil phase exists. Therefore, the cooling effect is lower than that of bearing center position.

From the abovementioned results, the authors considered that the internal flow of the oil-filler port influenced the temperature characteristics of starved lubrication conditions. Therefore, we focused on the calculation results in the oil-filler port under starved lubrication conditions.

4.4.2 Results in oil-filler port

Figure 14 shows the calculation results of the oil-filler port. **Figure 14(a)** indicates the results of the internal oil-filler port at the center of the bearing width of starved lubrication condition. **Figure 14(i-a)** indicates the volume fraction, while **Figure 14(i-b)** indicates the temperature. Moreover, **Figure 14(ii)** indicates the analytical results in the front view of the oil-filler port. From **Figure 14(ii)**, the temperature is high near the shaft, and the volume fraction decreases in that area. From the above, it is considered that the gas phase in this region is a circulating flow. In contrast, the gas phase exists in the wide area in the inside of the oil-filler port, while the temperature of the gaseous phase is smaller than the temperature of supply oil. Moreover, it is found that the temperature of oil is commensurate with the temperature of supply oil or less than. Furthermore, the temperature of the gaseous phase from the bearing clearance is about 40°C at the center of the oil-filler port. In **Figure 14(ii)**, the gaseous phase exists in the wide area in the inside of the oil-filler port as with **Figure 14(i)**, while it exists also in the oil-supply groove. The temperature of gaseous phase around the side end of the oil-supply groove is the same as the ambient atmosphere temperature set on the analysis; thus, it is found that outside air counterflows the oil-supply groove. From these results, in the case of the starved lubrication condition, it is considered that the outside air flows from
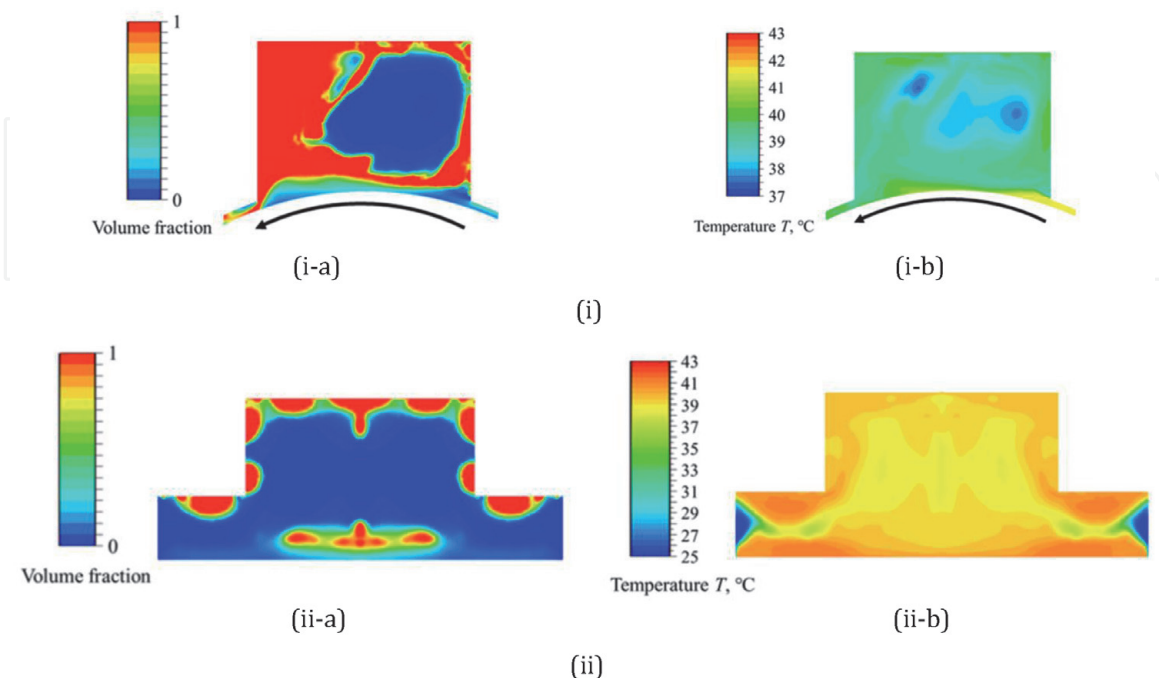

Figure 14.
Calculation results in the oil-filler port under starved lubrication conditions [2]. (i) Results in the center surface from the view of the side ((a) Volume fraction; (b) Temperature). (ii) Results in the front view ((a) Volume fraction; (b) Temperature).

the oil-supply groove and the side end of bearing cooled the supplied oil and the circulating flow; thus, the temperature of the center of bearing is controlled.

5. Conclusion

In this chapter, using a two-phase flow CFD analysis, the calculation of gaseous-phase areas in journal bearings under flooded and starved lubrication conditions was conducted, and the surface tension effect on multiphase flow CFD analysis of journal bearing especially generating the gaseous-phase area was studied.

As a result of comparing the calculation results and the experimental results, the VOF calculation considering the surface tension and vapor pressure was observed to be in good agreement under both lubrication conditions.

Furthermore, under starved lubrication, the calculation results of the interface of the oil film and gaseous phase during oil-film rupture agree rather well with experimental visualization result if they consider both vapor pressure and surface tension. While using these results, the effect of surface tension was discussed from the viewpoint of the Weber number, and it is concluded that the Weber number is strongly lower than one by using the supply oil speed as the representative speed and strongly influenced.

Moreover, thermal CFD analysis of a two-phase flow was conducted under two conditions of supply oil, and they were compared with the experiment. As a result, it is believed that in the case of the starved lubrication conditions, the air flowing outside of the oil-supply groove created a circulating flow; thus, the temperature in the bearing is controlled.

It is concluded that the two-phase VOF CFD analysis considering the vapor pressure and surface tension is applicable in reproducing the gaseous phase on the journal bearing.

Conflict of interest

The authors declare no conflict of interest.

Author details

Masayuki Ochiai*, Fuma Sakai and Hiromu Hashimoto
Department of Mechanical Engineering, Tokai University, Kanagawa, Japan

*Address all correspondence to: ochiaim@keyaki.cc.u-tokai.ac.jp

IntechOpen

References

[1] Ochiai M, Sakai F, Hashimoto H. Reproducibility of gaseous phase area on journal bearing utilizing multi-phase flow CFD analysis under flooded and starved lubrication conditions. Lubricants. 2019;**7**:74

[2] Sakai F, Ochiai M, Hashimoto H. Two-phase flow CFD analysis of temperature effects on oil supplied to small-bore journal bearing with oil supply groove. Tribology Online. 2018;**13**(5):232-240

[3] Hashimoto H, Ochiai M. Stabilization method for small-bore journal bearing utilizing starved lubrication. ASME Journal of Tribology. 2010;**132**:1-7

[4] Naruse Y, Ochiai M. Experimental study of safety supply flow rate on a small bore cylindrical journal sliding bearing. Journal of Advanced Science. 2012;**24**:24-28

[5] Heshmat H, Pinkus O. Performance of starved journal bearings with oil ring lubrication. ASME Journal of Tribology. 1985;**107**:23-31

[6] Gümbel L, Reibung und Schmierung im Maschinenbau. In: Everling E, editor. Berlin: Verlag von M. Krayn. 1925. VII + 240 S. Mit 37 Abb. Preis brosch. 12 M. ZAMM – Zeitschrift für Angewandte Mathematik und Mechanik [Internet]. 1927;**7**(5):415-415. Wiley; Available from: http://dx.doi.org/10.1002/zamm.19270070523

[7] Swift WH. The stability of lubricating films in journal bearings. In: Minutes of the Proceedings of the Institution of Civil Engineers, Vol. 233. London, UK: Thomas Telford-ICE Virtual Library; 1932. pp. 267-288

[8] Coyne JC, Elrod HG. Condition for the rupture of a lubricating film part i: Theoretical model. ASME Journal of Lubrication Technology. 1970;**92**:451-456

[9] Coyne JC, Elrod HG. Condition for the rupture of a lubricating film. Part II: New boundary conditions for Reynolds equation. ASME Journal of Lubrication Technology. 1971;**93**:156-167

[10] Ikeuchi K, Mori H. Hydrodynamic lubrication in seals with cavitation: 1st report, effect of cavity pressure on lubricating film. Bulletin of JSME. 1982;**25**:1002-1007 (in Japanese)

[11] Ikeuchi K, Mori H. An analysis of the lubricating films in journal bearings—Effects of oil supply condition on the static performance. Lubrication. 1982;**27**:533-540 (in Japanese)

[12] Boncompine R, Fillon M, Frene J. Analysis of thermal effects in hydrodynamics bearing. ASME Journal of Tribology. 1986;**108**:219-224

[13] Hatakenaka K, Tanaka M, Sizuki K. Thermo-hydrodynamic performance of journal bearings with partial reverse flow and finger-type cavitation being considered. Journal of Japanese Society of Tribologists. 2000;**45**:628-635 (in Japanese)

[14] Hashimoto H, Ochiai M. Experimental study on the stabilization of small-bore journal bearings by controlling starved lubrication and bearing orientation angle. ASME Journal of Tribology. 2009;**131**:011705

[15] Sakai F, Ochiai M, Hashimoto H. Stability characteristics and CFD analysis of two-phase flow of oil film journal bearing having two oil filler holes. Transactions of the JSME. 2017;**83**:16-00457 (in Japanese)

[16] Schnerr GH, Sauer J. Physical and numerical modeling of unsteady cavitation dynamics. In: Proceedings of the 4th International Conference on Multiphase Flow; New Orleans, LA, USA; 2001

[17] Ohta M, Sakai M, Shimada N, Honma S. Numerical Simulation of Multiphase Flow. Tokyo, Japan: Maruzen-Publishing; 2015 (in Japanese)

[18] Zhai LM, Luo YY, Wang ZW. Study about the influence of cavitation on the dynamic characteristics for the sliding bearing. IOP Conference Series: Materials Science and Engineering. 2015;**72**:1-10

[19] Dhande YD, Pande WD. Multiphase flow analysis of hydrodynamic journal bearing using CFD coupled fluid structure interaction considering cavitation. Journal of King Saud University - Engineering Sciences. 2016;**30**(4):345-354

[20] Egbers C, Gorenz P, Schmidt M, Wolf C. 3-D CFD simulation of the lubrication film in a journal bearing. Tribology International. 2008;**76**:40-47

[21] Olsson E, Kreiss G, Zahedi S. A conservative level set method for two phase flow II. Journal of Computational Physics. 2007;**225**:785-807

[22] Hirt CW, Nichols BD. Volume of fluid (VOF) method for the dynamics of free boundaries. Journal of Computational Physics. 1981;**39**:201-225

[23] Tryggvasona G, Bunner B, Esmaeelic A, Juricd D, Al-Rawahi D, Tauber W, et al. A front-tracking method for the computations of multiphase flow. Journal of Computational Physics. 2001;**169**: 708-759

[24] Bogdan RK, Abdollah AA. A Lattice-Boltzmann approach to fluid film lubrication. ASME Journal of Tribology. 2010;**132**(2):1-7

[25] Brackbill J, Douglas U, Koth B, Zemach C. A continuum method for modeling surface tension. Journal of Computational Physics. 1992;**100**: 335-335

[26] Tanaka M. Journal bearing performance under starved lubrication. Tribology International. 2000;**33**(3): 259-264

[27] Taura H, Kaneko S. Static characteristics of journal bearings under starved lubricating conditions. Transactions of the JSME. 2011;**77**: 3511-3521